1-1994

Measurement of the cross section for $\gamma\gamma \to p\bar{p}$

ARTUSO, M.; et al.

M. THULASIDAS
Singapore Management University, manojt@smu.edu.sg

ARTICLES

Measurement of the cross section for $\gamma\gamma \to p\bar{p}$

M. Artuso,[1] D. He,[1] M. Goldberg,[1] N. Horwitz,[1] R. Kennett,[1] G. C. Moneti,[1] F. Muheim,[1] Y. Mukhin,[1] S. Playfer,[1] Y. Rozen,[1] S. Stone,[1] M. Thulasidas,[1] G. Vasseur,[1] G. Zhu,[1] J. Bartelt,[2] S. E. Csorna,[2] Z. Egyed,[2] V. Jain,[2] P. Sheldon,[2] D. S. Akerib,[3] B. Barish,[3] M. Chadha,[3] S. Chan,[3] D. F. Cowen,[3] G. Eigen,[3] J. S. Miller,[3] C. O'Grady,[3] J. Urheim,[3] A. J. Weinstein,[3] D. Acosta,[4] M. Athanas,[4] G. Masek,[4] H. Paar,[4] M. Sivertz,[4] A. Bean,[5] J. Gronberg,[5] R. Kutschke,[5] S. Menary,[5] R. J. Morrison,[5] S. Nakanishi,[5] H. N. Nelson,[5] T. K. Nelson,[5] J. D. Richman,[5] A. Ryd,[5] H. Tajima,[5] D. Schmidt,[5] D. Sperka,[5] M. S. Witherell,[5] M. Procario,[6] S. Yang,[6] R. Balest,[7] K. Cho,[7] M. Daoudi,[7] W. T. Ford,[7] D. R. Johnson,[7] K. Lingel,[7] M. Lohner,[7] P. Rankin,[7] J. G. Smith,[7] J. P. Alexander,[8] C. Bebek,[8] K. Berkelman,[8] D. Besson,[8] T. E. Browder,[8] D. G. Cassel,[8] H. A. Cho,[8] D. M. Coffman,[8] P. S. Drell,[8] R. Ehrlich,[8] R. S. Galik,[8] M. Garcia-Sciveres,[8] B. Geiser,[8] B. Gittelman,[8] S. W. Gray,[8] D. L. Hartill,[8] B. K. Heltsley,[8] C. D. Jones,[8] S. L. Jones,[8] J. Kandaswamy,[8] N. Katayama,[8] P. C. Kim,[8] D. L. Kreinick,[8] G. S. Ludwig,[8] J. Masui,[8] J. Mevissen,[8] N. B. Mistry,[8] C. R. Ng,[8] E. Nordberg,[8] M. Ogg,[8,*] J. R. Patterson,[8] D. Peterson,[8] D. Riley,[8] S. Salman,[8] M. Sapper,[8] H. Worden,[8] F. Würthwein,[8] P. Avery,[9] A. Freyberger,[9] J. Rodriguez,[9] R. Stephens,[9] J. Yelton,[9] D. Cinabro,[10] S. Henderson,[10] K. Kinoshita,[10] T. Liu,[10] M. Saulnier,[10] F. Shen,[10] R. Wilson,[10] H. Yamamoto,[10] B. Ong,[11] M. Selen,[11] A. J. Sadoff,[12] R. Ammar,[13] S. Ball,[13] P. Baringer,[13] D. Coppage,[13] N. Copty,[13] R. Davis,[13] N. Hancock,[13] M. Kelly,[13] N. Kwak,[13] H. Lam,[13] Y. Kubota,[14] M. Lattery,[14] J. K. Nelson,[14] S. Patton,[14] D. Perticone,[14] R. Poling,[14] V. Savinov,[14] S. Schrenk,[14] R. Wang,[14] M. S. Alam,[15] I. J. Kim,[15] B. Nemati,[15] J. J. O'Neill,[15] H. Severini,[15] C. R. Sun,[15] M. M. Zoeller,[15] G. Crawford,[16] C. M. Daubenmier,[16] R. Fulton,[16] D. Fujino,[16] K. K. Gan,[16] K. Honscheid,[16] H. Kagan,[16] R. Kass,[16] J. Lee,[16] R. Malchow,[16] F. Morrow,[16] Y. Skovpen,[16,†] M. Sung,[16] C. White,[16] J. Whitmore,[16] P. Wilson,[16] F. Butler,[17] X. Fu,[17] G. Kalbfleisch,[17] M. Lambrecht,[17] W. R. Ross,[17] P. Skubic,[17] J. Snow,[17] P. L. Wang,[17] M. Wood,[17] D. Bortoletto,[18] D. N. Brown,[18] J. Fast,[18] R. L. McIlwain,[18] T. Miao,[18] D. H. Miller,[18] M. Modesitt,[18] S. F. Schaffner,[18] E. I. Shibata,[18] I. P. J. Shipsey,[18] P. N. Wang,[18] M. Battle,[19] J. Ernst,[19] H. Kroha,[19] S. Roberts,[19] K. Sparks,[19] E. H. Thorndike,[19] C. H. Wang,[19] J. Dominick,[20] S. Sanghera,[20] V. Shelkov,[20] T. Skwarnicki,[20] R. Stroynowski,[20] I. Volobouev,[20] and P. Zadorozhny[20]

(CLEO Collaboration)

[1] *Syracuse University, Syracuse, New York 13244*
[2] *Vanderbilt University, Nashville, Tennessee 37235*
[3] *California Institute of Technology, Pasadena, California 91125*
[4] *University of California, San Diego, La Jolla, California 92093*
[5] *University of California, Santa Barbara, California 93106*
[6] *Carnegie-Mellon University, Pittsburgh, Pennsylvania 15213*
[7] *University of Colorado, Boulder, Colorado 80309-0390*
[8] *Cornell University, Ithaca, New York 14853*
[9] *University of Florida, Gainesville, Florida 32611*
[10] *Harvard University, Cambridge, Massachusetts 02138*
[11] *University of Illinois, Champaign-Urbana, Illinois 61801*
[12] *Ithaca College, Ithaca, New York 14850*
[13] *University of Kansas, Lawrence, Kansas 66045*
[14] *University of Minnesota, Minneapolis, Minnesota 55455*
[15] *State University of New York at Albany, Albany, New York 12222*
[16] *Ohio State University, Columbus, Ohio 43210*
[17] *University of Oklahoma, Norman, Oklahoma 73019*
[18] *Purdue University, West Lafayette, Indiana 47907*
[19] *University of Rochester, Rochester, New York 14627*
[20] *Southern Methodist University, Dallas, Texas 75275*

(Received 1 September 1993)

A measurement of the cross section for $\gamma\gamma \to p\bar{p}$ is performed at two-photon center-of-mass energies between 2.00 and 3.25 GeV. These results are obtained using $e^+e^- \to e^+e^-p\bar{p}$ events selected from 1.31 fb^{-1} of data taken with the CLEO II detector. The measured cross section

*Permanent address: Carleton University, Ottawa, Canada K1S 5B6.
†Permanent address: INP, Novosibirsk, Russia.

is in reasonable agreement with previous measurements and is in excellent agreement with recent calculations based on a diquark model. However, leading order QCD calculations performed using the Brodsky-Lepage formalism are well below the measured cross section.

PACS number(s): 13.65.+i, 12.38.Qk, 13.60.Rj

I. INTRODUCTION

The production of hadronic final states through photon-photon interactions provides a unique laboratory for studying QCD. An interesting case is the two-photon production of proton antiproton pairs. Several authors [1–3] have presented calculations of the absolute cross section for $\gamma\gamma \to p\bar{p}$ which are performed within the framework developed by Brodsky and Lepage [4]. A remarkable feature of these calculations is that many of the nonperturbative components may be absorbed into the proton wave functions, thus exposing the perturbatively calculated matrix element. These calculations are to leading (fourth) order in the strong coupling constant and neglect the masses of the constituent quarks. As such, they are expected to be most reliable at large values of the two-photon center-of-mass energy (W), well above threshold.

The proton wave function may be modeled in a variety of ways. One of the most successful approaches is the use of QCD sum rules by Chernyak and Zhitnitsky [5]. Calculations incorporating their wave functions are generally in agreement with experimental measurement of quantities such as the proton's magnetic form factor and the decay rate for $J/\psi \to p\bar{p}$. The agreement between experiment and theory in the case of the reaction $\gamma\gamma \to p\bar{p}$ is not as satisfactory. The cross section obtained by convoluting the matrix element with the wave functions of Chernyak and Zhitnitsky is in disagreement with previous measurements [6–9]. The success of these wave functions in the calculation of other reactions has led to speculation that the source of this disagreement lies in the inability of previous experiments to explore the cross section with sufficient statistics at large enough values of W to be in the fully perturbative region.

An alternate approach towards the calculation of the $\gamma\gamma \to p\bar{p}$ cross section that has recently been taken is more suited towards smaller values of W. Anselmino *et al.* and Kroll *et al.* [10–12] have proposed a phenomenological model in which two of the valence quarks in each proton are treated as a quasielementary constituent (a diquark). The diquark model introduces form factors so that its predictions asymptotically approach those of the pure quark model of Brodsky and Lepage. Free parameters have been adjusted using data from elastic electron proton scattering so as to obtain an absolute prediction for the $\gamma\gamma \to p\bar{p}$ cross section. The lower range of applicability of the diquark model is about 2.5 GeV. Near this value of W, the predictions of the pure quark and the diquark models differ by one order of magnitude. The diquark model appears to be in approximate agreement with previous measurements, but a serious comparison cannot yet be made because data for values of W exceeding 2.5 GeV are quite limited. While a W of 2.5 GeV is considered low by theoretical standards, it is at the upper limit of present experimental sensitivity as the cross section for $\gamma\gamma \to p\bar{p}$ falls approximately as W^{-12} [8]. Thus, much larger data samples are necessary even to reach the lower range of applicability of the diquark theory. Such a data sample has been obtained using the CLEO II detector at the Cornell Electron Storage Ring (CESR).

We report herein a measurement of the cross section for $\gamma\gamma \to p\bar{p}$ for W between 2.00 and 3.25 GeV. This measurement is based on a data set comprising 1.31 fb^{-1} of electron-positron collisions obtained with the CLEO II detector. The detector operates at CESR, which has a beam energy of approximately 5.29 GeV. An electron-positron collider is also a photon-photon collider, as nearly real photons emitted by beam particles may interact. This is the origin of the events used in this study. The presence of two photon propagators in the amplitude for the $e^+e^- \to e^+e^-p\bar{p}$ reaction and the smallness of the electron mass ensure that the beam particles emitting the photons are scattered through angles so small that they may only rarely be detected. As a result, the net transverse momentum of the two-photon system is typically small, as is the energy visible to the detector. However, the energies of the photons are usually unequal, so that the final state particles are boosted toward the high rapidity regions of the detector. Because the luminosity of the data sample used in this analysis is three times larger than the luminosity of all previous experiments combined, our measurement has greater statistical precision and extends to higher values of W than previous measurements.

II. EXPERIMENTAL APPARATUS

The CLEO II detector [13] was designed to detect charged particles and photons with excellent efficiency and resolution. The charged particle tracking system, which surrounds a beryllium beam pipe, consists of a six layer straw tube detector, followed by a ten layer drift chamber and a 51 layer drift chamber. The outer drift chamber is instrumented to measure the specific ionization energy loss (dE/dx) from charged tracks. Surrounding the tracking system are a time-of-flight scintillation system and an electromagnetic calorimeter, the latter consisting of 7800 cesium iodide crystals. All of these detector systems are confined within a 1.5 T superconducting solenoidal magnet. Immediately outside the magnet cryostat are three layers of iron forming the flux return. Surrounding each layer of iron is a set of tracking chambers which provides muon detection.

This analysis makes use of two triggers [14]. One is designed to be efficient for low multiplicity events containing minimum ionizing particles. It requires at least

two candidate tracks in the tracking chambers, one with momentum transverse to the beam direction (p_t) greater than 0.4 GeV/c and the other with p_t greater than 0.2 GeV/c. It further requires hits in at least two nonadjacent time-of-flight counters and at least two deposits of energy greater than 0.1 GeV in the calorimeter; this final requirement is efficient for minimum ionizing particles. The other trigger is designed to be efficient for low multiplicity events that contain at least one high energy photon or electron. It requires at least two candidate tracks with p_t greater than 0.2 GeV/c, hits in at least two nonadjacent time-of-flight counters, and at least one energy deposit greater than 0.5 GeV in the calorimeter. This latter requirement is often met by antiprotons, which tend to annihilate and deposit significant amounts of energy in the calorimeter. Elements of these two triggers are redundant with those of other triggers, allowing for the measurement of their individual efficiencies from data.

III. EVENT SELECTION

The event selection is tailored to capitalize on the two-photon experimental signature while limiting contamination from background processes. Particular emphasis is placed on particle identification. This is because background events containing lighter particles preferentially populate the higher W region, which is the region of greatest interest.

Since the scattered electron and positron are undetected, we limit our study to events having exactly two oppositely charged tracks that satisfy one or both of the triggers described in the previous section. The largest source of such events is "single photon annihilation" in which the initial electron and positron annihilate with their energy reappearing in the form of a lepton pair. These events are suppressed by requiring that the sum of the magnitudes of the charged particle momenta be less than 8 GeV/c and that the total energy deposited in the calorimeter be less than 8 GeV.

A significant fraction of the remaining background events are due to collisions of beam particles with residual gas molecules within the vacuum chamber ("beam-gas" events) or with the beam pipe itself ("beam-wall" events). The contribution from these is limited by demanding that the tracks project to the interaction region. The small number of cosmic ray events remaining in the sample are suppressed by rejecting events in which the tracks are colinear. This removes only a very small number of signal events because of the boost of the two-photon center of mass. Since the boost is generally along the beam direction, the signal events will have small acoplanarity, defined as the supplement of the angle between the transverse momenta of the two tracks. In order to reject events involving the nonexclusive production of a proton-antiproton pair, events are only accepted if they have acoplanarity less than 0.1 rad. In addition, the magnitude of the vector sum of the transverse momenta of the two tracks (p_t^{event}) is required to be less than 0.2 GeV/c.

Most remaining background events are the result of other two-photon reactions, notably $\gamma\gamma \to e^+e^-$, $\mu^+\mu^-$, $\pi^+\pi^-$, and K^+K^-. Thus kinematics can provide no further assistance and we rely instead on the particle identification capabilities of CLEO II. We restrict the tracks to the central region of the detector ($|\cos\theta| < 0.7$) where the particle identification is optimal. The background from the reaction $\gamma\gamma \to \mu^+\mu^-$ is reduced by rejecting events in which either track in the drift chamber matches a track in the muon chambers. To reduce the contribution from the $\gamma\gamma \to e^+e^-$ reaction, events are discarded if either track has a value of E_{cal}/p near unity, where E_{cal} is the energy that is matched to the track as registered by the calorimeter and p is the measured momentum.

The measured dE/dx and time-of-flight information is combined for each track [6] to aid in suppressing any remaining nonproton backgrounds. A statistic is defined for a track to have an energy loss consistent with that expected for a given particle species:

$$\chi_j^{dE/dx} = \left[\left(\frac{dE}{dx}\right)^{\text{meas}} - \left(\frac{dE}{dx}\right)_j^{\text{expected}}\right] / \sigma_j^{dE/dx}, \quad j = e, \pi, K, p. \quad (1)$$

Here $\sigma_j^{dE/dx}$ is the dE/dx resolution measured as a function of momentum from data. A similar statistic, χ_j^{TF}, is defined for the time of flight. We require $|\chi_p^{dE/dx}| < 3$ and $|\chi_p^{\text{TF}}| < 3$. The likelihood ($\mathcal{L}$) that a track is of a particular species j is determined by combining these statistics:

$$\mathcal{L}_j = \exp\left\{-\frac{1}{2}\left[\left(\chi_j^{dE/dx}\right)^2 + \left(\chi_j^{\text{TF}}\right)^2\right]\right\}, \quad j = e, \pi, K, p. \quad (2)$$

The likelihoods for each particle species are combined to determine the normalized likelihood that a track is a proton:

$$\lambda_p = \frac{\mathcal{L}_p}{\mathcal{L}_e + \mathcal{L}_\pi + \mathcal{L}_K + \mathcal{L}_p}. \quad (3)$$

The power of this method of particle identification is demonstrated in Fig. 1, a two-dimensional histogram of λ_p for the positively and negatively charged tracks. Events satisfying all selection criteria discussed so far with the exclusion of the χ_p cuts are entered in the plot. The entries in the $(p, \bar{p})$ bin correspond to events in which one track is identified as a p and the other as a $\bar{p}$. The absence of significant enhancement at λ_p near 0.5 indicates that there is little ambiguity in identifying protons and antiprotons. Nearly all of the 2×10^5 entries are in the truncated bin marked (X^+, X^-). The majority of the entries in this bin correspond to two-photon produced pion and muon pairs. The entries in the (p, X^-) bin are generally consistent with being beam-gas events in which a proton is accompanied by a particle other than an antiproton. The small enhancement in the $(X^+, \bar{p})$

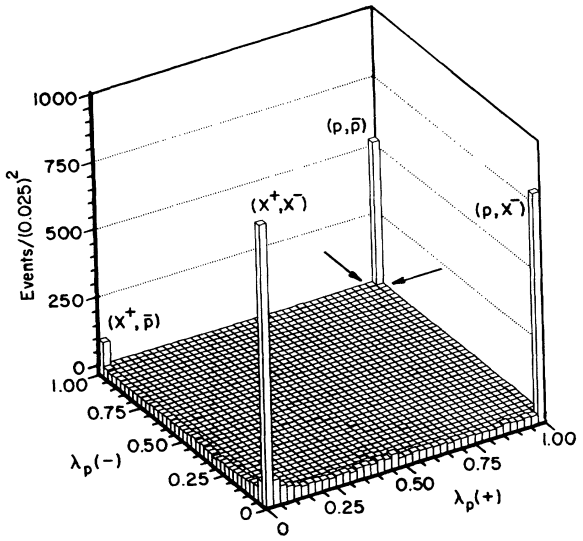

FIG. 1. A two-dimensional histogram of the normalized likelihood for the proton hypothesis for the positively charged [$\lambda_p(+)$] and negatively charged tracks [$\lambda_p(-)$]. Events from the data that pass all cuts prior to the proton selection cuts are entered. The bin at (0,0) contains approximately 2×10^5 entries and is truncated at 1000. The cuts on the quantities are indicated by arrows.

bin indicates that there is little feed-down from reactions involving the nonexclusive production of $p\bar{p}$ pairs, such as $e^+e^- \to e^+e^-p\bar{p}\pi^+\pi^-$. A total number of 484 events from the signal reaction are selected by the requirement that λ_p be greater than 0.95 for both tracks. These $e^+e^- \to e^+e^-\gamma^*\gamma^* \to e^+e^-p\bar{p}$ candidate events comprise the sample with which the cross section for $\gamma\gamma \to p\bar{p}$ is measured.

IV. EVENT SIMULATION

A sample of simulated events is used to determine the effective photon-photon luminosity and the acceptance for the reaction of interest. Both quantities are determined as functions of W and θ^*, where the latter is the angle between the $p\bar{p}$ axis and the $\gamma\gamma$ axis in the photon-photon center-of-mass frame. The photon flux is generated using the formalism of Budnev *et al.* [15]. The hadronic component of each photon is modeled using a ρ form factor. This is consistent with a previous measurement [8] of the form factor. In addition, the assumption is made that only transversely polarized photons contribute to the cross section. The $\gamma\gamma \to p\bar{p}$ cross section is modeled using [8]

$$\frac{d\sigma^{\mathrm{MC}}_{\gamma\gamma\to p\bar{p}}}{d|\cos\theta^*|} = \frac{a}{W^b}\sqrt{1-\left(\frac{2m_p}{W}\right)^2}. \qquad (4)$$

The values of a and b are taken to be 1.5×10^5 nb GeV^{12} and 12, respectively, which are in approximate agreement with previous experimental measurements [8]. The scaling as $1/W^b$ is derived loosely from the perturbative calculations [1], while the final factor accounts for two-particle phase space. The protons are generated isotropically in the photon-photon center of mass. The exact form of this ansatz [Eq. (4)] is unimportant since it cancels to a large extent in the extraction of the cross section. Nevertheless, the form chosen here reflects the gross features expected.

The detector's response is simulated using a Monte Carlo program based on GEANT [16], which includes the electromagnetic and hadronic interactions of particles with detector materials. The simulation of many detector components is calibrated from data. The effect of noise in the detector is modeled by embedding events from data taken with a random trigger into the simulated events. In general, the data and Monte Carlo events show good agreement in the quantities used for event selection. For example, Fig. 2 is a histogram of p_t^{event} for events from the data and Monte Carlo samples that pass all selection cuts. The Monte Carlo sample is scaled so as to have an equal number of selected events. The only exception to this good agreement between data and Monte Carlo simulation involves the modeling of the annihilation of antiprotons. This can be seen in Fig. 3, which is a histogram of E_{cal}/p for the negatively charged track. Events that pass all selection criteria are entered from the data and Monte Carlo samples; the latter is normalized to have the same number of entries as the former. The discrepancy in the first bin is due to a slightly softer momentum spectrum of the Monte Carlo sample which results in an overestimate of the number of particles that do not reach the calorimeter and consequently have E_{cal}/p equal to zero. In addition, the Monte Carlo simulation underestimates the amount of energy that the antiprotons deposit in the calorimeter. The region of E_{cal}/p near 1.0 is excluded by a cut designed to reject electrons as described in Sec. III. Removing the cut causes no enhancement near 1.0 which would be indicative of background. The uncut distributions for data and Monte Carlo samples

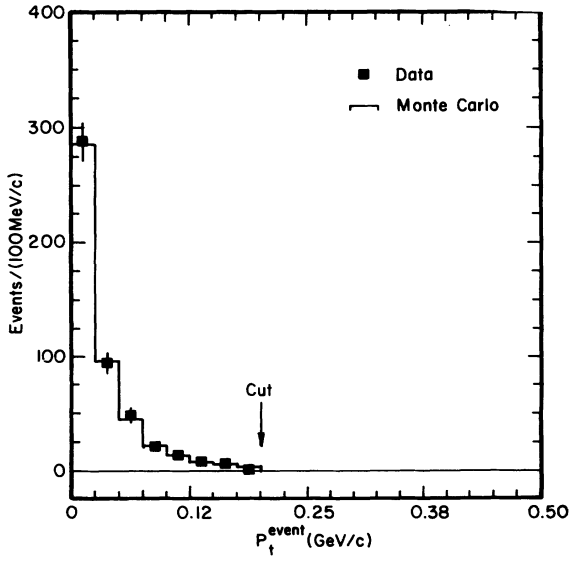

FIG. 2. Histogram of the magnitude of the vector sum of the transverse momenta of the two tracks (p_t^{event}) for events from the data and Monte Carlo samples that pass all selection cuts. The Monte Carlo sample is scaled so as to have an equal number of selected events. The cut on p_t^{event} is indicated.

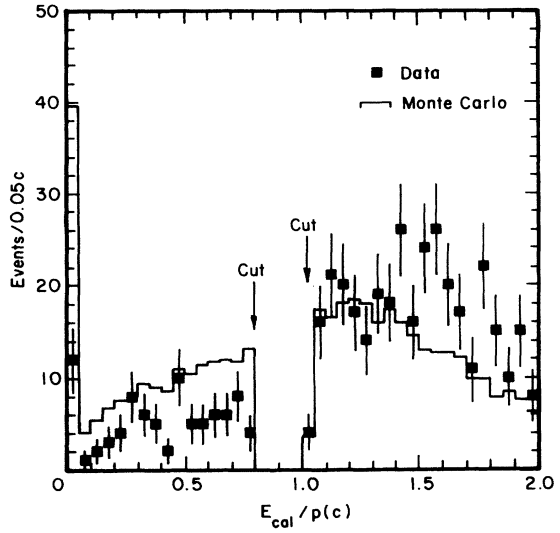

FIG. 3. Histogram of E_{cal}/p for the negatively charged track. Events from the data and Monte Carlo samples passing all selection cuts are entered in the plot. The Monte Carlo sample is scaled so as to have an equal number of selected events. The cuts on E_{cal}/p are indicated.

are relatively flat across this region. The efficiencies of the cut as determined using data and Monte Carlo samples are in good agreement with one another. In addition, these efficiencies agree with one determined from a sample of $\Lambda \to \bar{p}\pi^+$ decays in hadronic events when the antiprotons are restricted to the same momentum range. Although the effect of the discrepancy between the antiproton annihilation energy spectrum of the data and Monte Carlo samples on the determination of the efficiency for the E_{cal}/p cut on the antiproton is rather small, its effect on the trigger efficiency is non-negligible. This is because the trigger efficiency increases rapidly in the region where the discrepancy is largest. The Monte Carlo simulation tends to underestimate the efficiency of the trigger component that requires a 0.5 GeV energy deposit in the calorimeter (see Sec. II). The redundancy of this component with others is exploited, allowing for the overall trigger efficiency determined from the Monte Carlo samples, which is 70%, to be corrected based on measurements from data. The correction factor is largest at low W, where it is 1.2; above 2.3 GeV, the correction is negligible. The acceptance (the fraction of raw signal events that pass all event selection criteria) is $2.5 \pm 0.3\%$, with most of the loss being due to the tendency for the particles to be produced with low momentum and at small angles with respect to the beam axis.

V. RESULTS

Because the acceptance is a function of both W and $|\cos\theta^*|$, we divide the event sample into two-dimensional bins of these two variables. The variable W is measured as the invariant mass of the two charged particles taken as protons, while θ^* is taken to be the angle between the proton's momentum and the electron beam direction in the photon-photon center-of-mass frame. The differential cross section in each two-dimensional bin is extracted using

$$\frac{d\sigma_{\gamma\gamma\to p\bar{p}}}{d|\cos\theta^*|} = \left(\frac{N_{\rm data}}{N_{\rm MC}\delta}\right)\left(\frac{\mathcal{L}^{\rm MC}_{e^+e^-}}{\mathcal{L}^{\rm data}_{e^+e^-}}\right)\left(\overline{\frac{d\sigma^{\rm MC}_{\gamma\gamma\to p\bar{p}}}{d|\cos\theta^*|}}\right). \quad (5)$$

The first factor is the ratio of the number of events in the data that pass the event selection criteria to the number that pass in the Monte Carlo simulation. The δ factor accounts for the tendency of the Monte Carlo simulation to underestimate the calorimeter trigger efficiency for low momentum antiprotons. As determined from data, the value of δ is 1.2 for W between 2.0 and 2.3 GeV and is 1.0 for larger values of W. The second factor in Eq. (5) is the ratio of the integrated e^+e^- luminosities, which are $1.31\,\text{fb}^{-1}$ for data and $93.8\,\text{fb}^{-1}$ for Monte Carlo samples. The last factor is the ansatz of Eq. (4) averaged over the appropriate two-dimensional bin. The boost of the two-photon center of mass in combination with our restriction of the two tracks to the central region of the detector results in a very small acceptance for large values of $|\cos\theta^*|$. Thus we restrict our measurement of the cross section to the region $|\cos\theta^*| < 0.6$.

Measurements of the differential cross section in two-dimensional bins of W and $|\cos\theta^*|$ are summed over $|\cos\theta^*|$ (from 0.0 to 0.6) in order to obtain the cross section for a given W bin. Figure 4 is a plot of the resulting cross section for $\gamma\gamma \to p\bar{p}$ as a function of the two-photon center-of-mass energy. Above threshold, the cross section reaches a maximum of 5.8 nb near 2.1 GeV. It then decreases by about a factor of 50 as W increases to 3.2 GeV, above which energy there are no more events detected. Figure 5 is a plot of the differential cross section for two different ranges of W. For the low W range

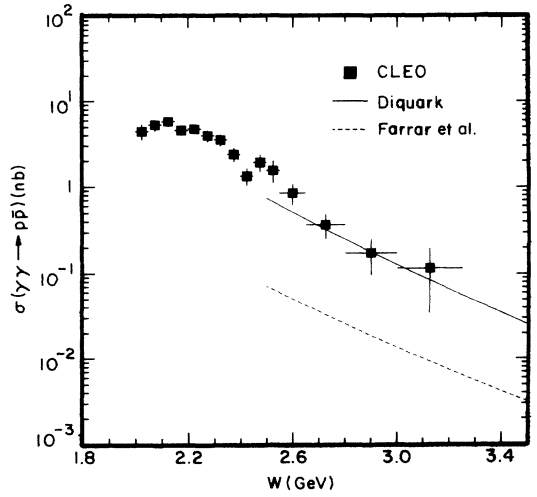

FIG. 4. Measured cross section for $\gamma\gamma \to p\bar{p}$ as a function of W. The results of two theoretical calculations are also shown. Experimental and theoretical results are restricted to the range of $|\cos\theta^*| < 0.6$.

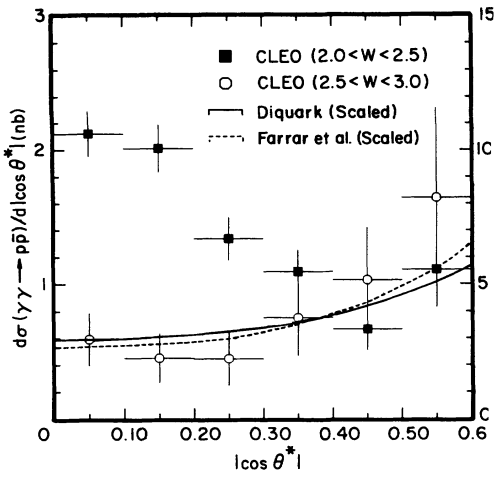

FIG. 5. Measured differential cross section for $\gamma\gamma \to p\bar{p}$ as a function of $|\cos\theta^*|$ for two ranges of W: $2.0 < W < 2.5$ GeV (left scale) and $2.5 < W < 3.0$ GeV (right scale). The results of two theoretical calculations are also shown. The normalization of each is scaled to agree with the high W measurement.

of 2.0 to 2.5 GeV, the average value of W is 2.2 GeV; while for the high W range of 2.5 to 3.0 GeV, the average is 2.6 GeV. The indicated errors in both figures are purely statistical.

There are five principal sources of systematic uncertainty for the measurement: model dependence, trigger efficiency, particle identification efficiency, background from feed-down, and background from particle misidentification. The largest source of uncertainty involves our choice of using a ρ form factor in the modeling of the hadronic component of the photons in the Monte Carlo event generator. Removing the ρ form factor has the effect of lowering the measured cross section by about 30%. This modeling uncertainty is, however, a theoretical uncertainty and not an actual measurement error. The dominant source of measurement systematic error has to do with the trigger efficiency, in particular the calorimeter efficiency because of the problem with modeling the annihilation of antiprotons. For W below 2.3 GeV, where the trigger efficiency is changing most rapidly, the systematic error due to trigger efficiency is about 10%. For large values of W the systematic error is dominated by the particle identification efficiency, which contributes about 6%. The contribution of background to the final event sample is determined to be at the 1% level. Contributions are negligible from reactions in which particles are misidentified as protons. The major source of background is feed-down from the reaction $\gamma\gamma \to p\bar{p}\pi^+\pi^-$ in which the pions are undetected. The contribution from such feed-down is estimated by studying events in which only a $\bar{p}$ and π^- are detected. Neglecting the theoretical uncertainty associated with our use of the ρ form factor, the combined systematic error is 10% for the entire range of W.

VI. DISCUSSION

Two theoretical curves are shown in Fig. 4. The dashed curve is based on the leading order QCD calculation of the $\gamma\gamma \to p\bar{p}$ matrix element performed by Farrar *et al.* [1], which agrees with the calculation performed by Millers and Gunion [2]. The prediction utilizes a running coupling constant and incorporates the wave function of Chernyak and Zhitnitsky. The solid curve is a result of calculations by Kroll *et al.* [12] performed in the context of a diquark model. While the shapes of the two theoretical curves are quite similar, the normalizations are significantly different. The prediction of Farrar *et al.* is about an order of magnitude below the measurement. The discrepancy is most likely due to the inapplicability of the calculation at values of W that are so close to threshold. Four possible sources for this inapplicability are the following: the fact that the calculation is only done to leading order, the perturbative nature of the calculation, the omission of the quark masses in the computation of the matrix element, and the possible presence of broad resonances in the $p\bar{p}$ mass spectrum. There is excellent agreement between the absolute predictions of the diquark model and our measurement. The diquark model is particularly well suited for the moderately large values of W reached by our measurement.

Figure 5 contains two theoretical predictions [1,17] for the angular dependence of the cross section. For the purpose of comparison, the normalization of each is scaled so as to agree with the high W measurement. This is possible because the predicted differential cross sections are weakly dependent on W. There is good agreement between the shapes of both theoretical curves and our measurement of the differential cross section for the W range of 2.5 to 3.0 GeV. The behavior of the $|\cos\theta^*|$ dependence of the cross section at the high W range is in marked contrast to the angular dependence for values

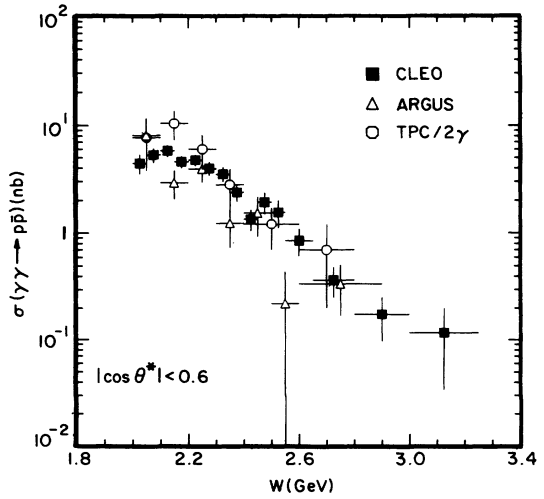

FIG. 6. Measured cross section for $\gamma\gamma \to p\bar{p}$ as a function of W. CLEO results are plotted along with those of ARGUS and TPC/2γ. All results are restricted to the range of $|\cos\theta^*| < 0.6$.

of W closer to threshold ($2.0 < W < 2.5\,\mathrm{GeV}$), where nonperturbative and higher twist effects are expected to play a larger role.

The CLEO measurement of the cross section is compared to the two most recent measurements [8,9] in Fig. 6. Except for the data points at very low W, the agreement between CLEO and TPC/2γ is excellent. The ARGUS results have central values that are somewhat lower, but agree within errors. There is reasonably good agreement between the CLEO measurement and those of JADE [7] and TASSO [6], which are not shown in the figure. The CLEO measurement of the angular dependence of the cross section is also in reasonable agreement with previous measurements [6–9]. The CLEO measurements of both the angular and the W dependence of the cross section are of significantly higher statistical precision than previous measurements and extend to larger values of the two-photon center-of-mass energy.

VII. CONCLUSION

We have used a sample of $e^+e^- \to e^+e^- p\bar{p}$ events to measure the cross section for $\gamma\gamma \to p\bar{p}$. The measurement is well above the results of a lowest order QCD calculation performed by Farrar *et al.* [1] within the framework developed by Brodsky and Lepage [4]. The diquark model of Kroll *et al.* [12] is in excellent agreement with our measurements.

The CLEO measurement is in reasonable agreement with all previous measurements [6–9]. Because of the large luminosity of the data sample, our measurement is of higher statistical precision and extends to larger values of W. Because the cross section is so strongly dependent on W, a measurement that extends to significantly larger values of W will most likely have to wait until the advent of a B factory.

ACKNOWLEDGMENTS

We gratefully acknowledge the effort of the CESR staff in providing us with excellent luminosity and running conditions. J.P.A. and P.S.D. thank the PYI program of the NSF, I.P.J.S. thanks the YI program of the National Science Foundation, G.E. thanks the Heisenberg Foundation, K.K.G. and A.J.W. thank the SSC Laboratory program of Texas National Research Laboratory Commission, K.K.G., H.N.N., J.D.R., and H.Y. thank the OJI program of the U.S. Department of Energy, and P.R. thanks the Alfred P. Sloan Foundation for support. This work was supported by the National Science Foundation and the U.S. Department of Energy.

[1] G. Farrar *et al.*, Nucl. Phys. **B259**, 702 (1985); **B263**, 746(E) (1986).
[2] D. Millers and J. Gunion, Phys. Rev. D **34**, 2657 (1986).
[3] T. Hyer, Phys. Rev. D **47**, 3875 (1993).
[4] S.J. Brodsky and G.P. Lepage, Phys. Rev. D **22**, 2157 (1980).
[5] V.L. Chernyak and I.R. Zhitnitsky, Nucl. Phys. **B246**, 52 (1984).
[6] TASSO Collaboration, M. Althoff *et al.*, Phys. Lett. B **130**, 449 (1983).
[7] JADE Collaboration, W. Bartel *et al.*, Phys. Lett. B **174**, 350 (1986).
[8] TPC/2γ Collaboration, A. Aihara *et al.*, Phys. Rev. D **36**, 3506 (1987).
[9] ARGUS Collaboration, H. Albrecht *et al.*, Z. Phys. C **42**, 543 (1989).
[10] M. Anselmino *et al.*, Int. J. Mod. Phys. A **4**, 5213 (1989).
[11] P. Kroll *et al.*, Int. J. Mod. Phys. A **6**, 4107 (1991).
[12] P. Kroll *et al.*, Phys. Lett. B **316**, 546 (1994).
[13] CLEO Collaboration, Y. Kubota *et al.*, Nucl. Instrum. Methods Res. Ser. A **320**, 66 (1992).
[14] CLEO Collaboration, C. Bebek *et al.*, Nucl. Instrum Methods Res. Ser. A **302**, 261 (1991).
[15] V.M. Budnev *et al.*, Phys. Rep. **15C**, 181 (1975).
[16] R. Brun *et al.*, GEANT 3.14, Report No. CERN DD/EE/84-1 (unpublished).
[17] M. Schürmann (private communication).